THE GEOLOGICAL SOCIETY OF AMERICA®

The minimum scale of grooving on faults

Thibault Candela[1,2]* and Emily E. Brodsky[1]
[1]Department of Earth and Planetary Sciences, University of California–Santa Cruz, 1156 High Street, Santa Cruz, California 95064, USA
[2]TNO, Geological Survey of The Netherlands, P.O. Box 80015, 3508 TA Utrecht, Netherlands

ABSTRACT

At the field scale, nearly all fault surfaces contain grooves generated as one side of the fault slips past the other. Grooves are so common that they are one of the key indicators of principal slip surfaces. Here, we show that at sufficiently small scales, grooves do not exist on fault surfaces. A transition to isotropic roughness occurs at 4–500 μm. Although the scale of the transition can vary even between locales on a single fault, the aspect ratio of the roughness at the transition is well defined for a given fault. We interpret the transition between grooved and ungrooved scales as a transition in deformation mode of asperities on the slip surface. Grooves can form when a hard indenter slides past a softer surface. At small scales, the asperities appear to yield plastically and therefore do not generate grooves as hard indenters. The plastic yielding can be a consequence of the high shear strains required to deform the surfaces at small scales where the aspect ratio (roughness) is high. The transition to plastic yielding is predicted to occur at a specific aspect ratio for each fault, as observed. The new observation both shows a limit to one of the most commonly observed features of faults and suggests a change in the mode of failure of faults as a function of scale.

INTRODUCTION

Localized, cohesive slip surfaces exist in fault zones both abutting and occasionally embedded in the gouge layer (Fig. 1). Geologists as early as Charles Lyell have noted that fault surfaces are generally covered with grooves elongated in the direction of slip (Lyell, 1871). Slickenlines are used to identify faults, infer kinematics, and calculate the stress state. Their existence helps to reinforce the interpretation of the slip surfaces as important loci of slip within the wider fault zones. Studies have improved our understanding of grooving by taking topographic data of either profiles on fault slip surfaces or, using more recent technology, over entire exposed fault surfaces (e.g., Power and Tullis, 1991; Sagy et al., 2007). As expected from the ubiquity of grooving, the quantitative data show that over scales from millimeters to tens of meters, the average variation of the surface height is greater on profiles perpendicular to slip than along profiles parallel to slip (Fig. 1; Power and Tullis, 1991; Renard et al., 2006). These observations have been used to infer mechanisms of fault resistance and wear (Scholz, 1988; Fang and Dunham, 2013; Brodsky et al., 2016).

In this paper, we report that grooves only exist on natural faults at macroscopic scales. At the submillimeter scale, we find a minimum scale of grooving on natural faults. The same observation holds for faults generated in laboratory experiments; therefore, the observation is not an artifact of weathering or preservation. We also explore the mechanical origins of this limit. We show that the minimum grooving scale corresponds to a particular aspect ratio of the surface roughness, and we interpret the aspect ratio as evidence for plastic failure of asperities. Because asperity failure is part of the microscopic process controlling friction, we finish the paper by exploring the implications for friction by comparing the minimum grooving scale with the slip weakening distance, where both measurements are available for previous laboratory experiments. We conclude that the laboratory data are consistent with both values being controlled by the plastic failure of asperities, and therefore the minimum grooving scale may be evidence for the same process occurring on natural faults.

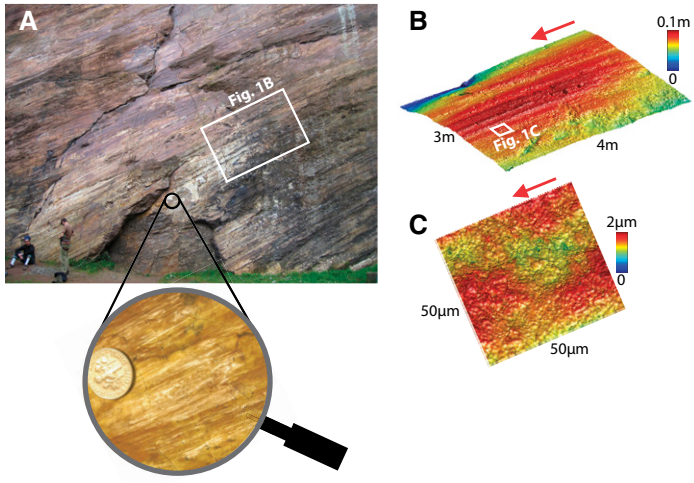

Figure 1. Field-scale roughness of fault surfaces. A: Example of an exhumed slip surface (Corona Heights fault, San Francisco, California) showing grooves elongated in the slip direction. B: Topographic map of this fault acquired by a lidar instrument. C: Topographic map of a sample of this fault acquired by a white light interferometer. Red arrows indicate slip direction. Grooves visible at the field scale in B are not observed at the finer scale in C.

OBSERVATION OF THE MINIMUM SCALE OF GROOVING

We measured the topography of slip surfaces from natural and experimental faults at scales of 1 μm to several millimeters using three different and complementary white light interferometers (see instrument descriptions in the GSA Data Repository[1]). Like most natural surfaces, faults have scale-dependent roughness. Therefore, a scale-dependent method such as Fourier analysis is required to quantify the topographic information. We used the same method as developed for field-scale digital topographic data on the submillimeter-scale data to define the minimum scale of grooving (Sagy et al., 2007; Candela et al., 2012). For each sampled region, the average Fourier spectrum was computed in the slip-parallel and slip-perpendicular directions. The power spectral density at a given wavelength is a measure of the roughness at that scale.

At the longest wavelengths measured by the white light interferometers, the spectra have lower roughness in the slip-parallel direction than the slip-perpendicular direction, like the field-scale observations (Fig. 2). Previous works have referred to this orientation dependence of roughness as anisotropy, and the behavior is found again on the fault surfaces here (Lee and Bruhn, 1996). However, at smaller scales, the slip-parallel

*E-mails: tcandela@ucsc.edu; thibault.candela@tno.nl

[1]GSA Data Repository item 2016196, descriptions of techniques and individual faults, is available online at www.geosociety.org/pubs/ft2016.htm, or on request from editing@geosociety.org.

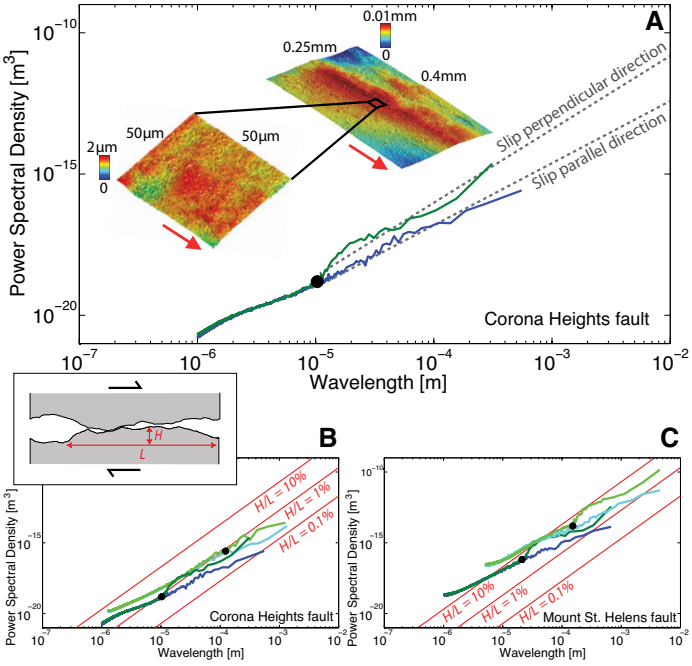

Figure 2. Minimum scale of grooving measured with Fourier spectral analysis. A: Example of slip-parallel and slip-perpendicular spectra obtained from one white light interferometer topographic map of the Corona Heights fault (San Francisco, California). Inset: Magnification of topographic map shows roughness isotropy at small scales in the spatial domain. The scale at which spectra coincide defines the minimum grooving scale (dark-filled circle). B: Spectra from multiple locales on the Corona Heights fault. Red reference lines show trends for constant aspect ratio *H*/*L*. Inset: Cartoon illustrates roughness geometry, where *H* is the average asperity height at length scale *L*. C: Same as B for Mount St. Helens (Washington, USA) fault. For each fault in B and C, minimum grooving scale varies between samples; however, the aspect ratio at the minimum grooving scale is constant.

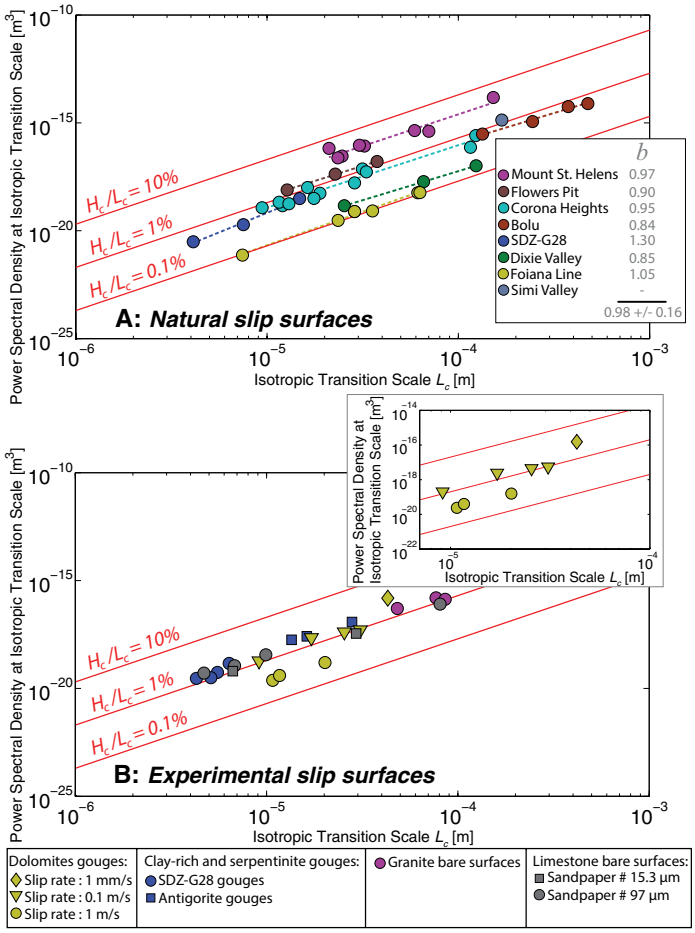

Figure 3. Compilation of the minimum scale of grooving for (A) natural and (B) experimental fault surfaces. Each symbol corresponds to the minimum grooving scale determined for each individual topographic map of either a natural fault or experimental surface. Each set of minimum grooving scales can be fit by a power law of the form $H_c = AL_c^b$ (dashed lines; H_c is the average asperity height at the minimum grooving scale L_c). The best-fit power-law roughness exponents *b* are close to one (inset of A) and indicate that each fault can be characterized by a single critical aspect ratio H_c/L_c.

and slip-perpendicular spectra coincide. At large scales, the surfaces are anisotropic; at small scales, they are isotropic.

The wavelength at which the spectra coincide defines the minimum scale of grooving for each measured map. We call this minimum grooving scale L_c, and by definition it marks the transition between anisotropic and isotropic roughness. We measured L_c on 42 topographic maps of eight different natural faults spanning a range of lithologies and faulting histories. We supplemented the data with 24 topographic maps of eight experimental faults (Fig. 3; see the Data Repository for fault descriptions).

The delineation of anisotropic and isotropic regimes introduced here is consistent with the only previously published extremely small-scale measurements of roughness. Atomic force microscopy (AFM) data showed the isotropic regime for a single carbonate fault, but it did not extend to large enough scales to capture the transition (Siman-Tov et al., 2013). Other AFM work showed nanofibers, which have smaller aspect ratios and are distinct from the deeper grooves studied here (Verberne et al., 2014).

Laboratory experiments in controlled conditions also produce grooves. We examined surfaces provided by several groups from frictional experiments using a variety of compositions and slip speeds (Goebel et al., 2013; Moore et al., 2012; Tisato et al., 2012; Fondriest et al., 2013; see the Data Repository for experiment descriptions). In some experiments, the starting material was powder, and cohesive slip surfaces were generated over the course of the experiment. These samples allowed us to study slip surfaces even for gouge-filled systems.

The samples from laboratory experiments are grooved at large scales, but they are ungrooved at sufficiently small scales, as was observed for the field samples (Figs. DR12–DR15 in the Data Repository). The consistency between the field and laboratory data demonstrates that the minimum grooving scale is generated by the mechanics of slip and is not a secondary process such as weathering.

MINIMUM GROOVING SCALE OCCURS AT CRITICAL ASPECT RATIO

Now that we have established the existence of minimum scale of grooving, we move on to identifying the mechanical controls on its existence. As a first step, we measured the average asperity height at the minimum grooving scale so that we could compare the roughness at the observed scales of L_c.

The power spectral density can be transformed to average asperity height to provide an interpretation in the spatial domain. For a given observation length L, the average asperity height is the integral of the power over wavelengths up to L. A power-law fit to the spectrum implies that the surface can be well described as a self-affine fractal surface. The average asperity height H is related to L by the power-law scaling $H = KL^{\zeta}$, where ζ is the Hurst exponent, which is sometimes called the roughness exponent, and K is a constant prefactor. For the extant fault data, ζ is <1, which means that the aspect ratio H/L increases with decreasing scale (Candela et al., 2012; Brodsky et al., 2016). This mathematical

formalism captures the fact that slip surfaces appear as smooth surfaces at large scale and rough at small scales.

We used this transformation to measure the average asperity height H_c at the observed minimum grooving scale L_c for each sample (Figs. 2B and 2C). For each fault, the observed minimum grooving scale varied between samples and even locations on the same sample. Because L_c varies, it cannot be related to a single intrinsic length scale of the rock, such as grain size. However, all samples on a given fault were consistent with a single aspect ratio H_c/L_c measured at the minimum scale of grooving (Figs. 2B, 2C, and 3). The consistency of H_c/L_c on each fault is distinct from the behavior of H/L overall. As expected based on the previous discussion of the Hurst exponent $\zeta < 1$, Figure 2 shows that H/L increases with decreasing scale for each fault. In contrast, the aspect ratio at the minimum grooving scale remains constant. For the laboratory samples, the minimum grooving scale L_c is defined by a single value of H_c/L_c (Fig. 3B). Again, the laboratory samples provide an important check on possible complications in the geological samples.

PLASTIC DEFORMATION DURING SHEARING

Next, we investigated why the minimum scale of grooving occurs at a specific aspect ratio for each fault. The aspect ratio H/L can be interpreted in terms of shear strain required for asperities to flatten (Scholz, 1988; Brodsky et al., 2016). As the two facing slip surfaces start to slide, asperities collide. The asperities must flatten or yield to pass each other. For a flattened asperity, the displacement normal to the surface H is accommodated over the asperity length L (Fig. 2B). The ratio H/L is therefore proportional to the shear strain required for flattening. This interpretation of aspect ratio H/L as strain is supported by rigorous analyses for elastic media and more general rheologies (Oyen and Cook, 2009; Brodsky et al., 2016). As discussed already, for faults, as the scale L decreases, the asperity aspect ratio H/L becomes larger, and the asperities steepen. Therefore, the shear strain required to accommodate the movement of colliding asperities increases with decreasing scale.

Once the asperities reach a critical aspect ratio H_c/L_c, the elastic shear strain reaches a critical value, and grooving does not occur because plastic yielding occurs instead. Engineering studies address plastic deformation on rough surfaces by comparing the elastic stress required to shear an asperity to the hardness of the material (Greenwood and Williamson, 1966; Johnson et al., 1985; Hyun et al., 2004; Williams, 2005). These works predict that sheared asperities deform plastically if $2/3\ E'H/L > \mathcal{H}$, where E' is the modified Young's modulus, and $\mathcal{H}$ is the hardness. The transition to plasticity, corresponding to the minimum grooving scale, should occur at the critical aspect ratio $H_c/L_c \sim 2/3(\mathcal{H}/E')$. Typical values of $\mathcal{H}$ and E' from nano-indentation testing on quartz are ~9 GPa and 90 GPa, respectively, and on calcite are ~2 GPa and 70 GPa (Brace, 1963; Oliver and Pharr, 1992; Broz et al., 2006). The corresponding predicted aspect ratios at the plastic transition for quartz and calcite are 7% and 2%, respectively. These values fall in the range of critical aspect ratios measured at the minimum grooving scale (0.1%–8%; Fig. 3). We conclude that interpretation of L_c as a plastic transition scale controlled by the roughness is consistent with typical material properties.

Asperity failure can still occur within the elastic regime, but it occurs brittlely, rather than plastically. Brittle failure requires that deformational strain energy is accumulated rather than dissipated immediately; therefore, the elastic regime is commonly associated in seismology with brittle failure (MacElwane, 1936). Grooving is the hallmark of abrasional wear dominated by brittle failure (Engelder and Scholz, 1976; Zum-Gahr, 1987). At small scales, brittle failure is suppressed on fault surfaces, and adhesive wear dominates. Therefore, L_c may be identified with a brittle-plastic transition. This identification is supported by thin section evidence of plasticity at small scales such as bands of preferred crystallographic orientation and sintering of the fine particles coating the slip surfaces on many of the faults studied (see the Data Repository for descriptions).

The interpretation of the minimum grooving scale as the plastic transition explains the variability of L_c and the consistency of H_c/L_c for each fault. For any given fault, the overall roughness (vertical position of the spectra in Fig. 2) differs between locales on the fault. This variability is also observed in the field-scale measurements (Candela et al., 2012). Each topographic map samples a portion of the fault surface that imperfectly captures the mean power. However, the material properties $\mathcal{H}$ and E' demand a well-defined value of H_c/L_c everywhere on the fault, as observed (Figs. 2B, 2C, and 3). Because H_c/L_c is well defined, grooving appears at different scales depending on the local roughness of each topographic map. In other words, H is a statistical quantity with a distribution of values; H_c/L_c is deterministically controlled by the material properties.

Interestingly, the experiment with the highest slip rate (1 m/s) had a lower value of H_c/L_c than the other laboratory experiments on the same material. The implication is that the high-slip-rate experiment yielded plastically at a lower critical strain. A low yield threshold would be expected for high-velocity experiments where thermal energy weakens asperities (Di Toro et al., 2011).

In summary, grooving generally occurs when hard indenters collide with softer material. If an indenter yields plastically, it is no longer hard, and no grooving results. Therefore, at high enough aspect ratios for plastic deformation, grooving is not favored. Since fault surfaces are rougher (have higher aspect ratios) at small scales, the small-scale roughness will preferentially yield plastically and not create grooves.

IMPLICATIONS FOR FRICTION

The change from dominantly brittle to plastic deformation as a function of scale is important for defining the asperity size that governs the frictional behavior (Engelder and Scholz, 1976). In the plastic regime, the deformed asperities can adhere to the opposite side of the fault and define the real area of contact between surfaces microscopically (Bowden and Tabor, 1950; Greenwood and Williamson, 1966; Williams, 2005). At larger scales, the abrasional grooves indicate that brittle failure occurs on the fault. We infer that both brittle failure and plastic asperity failure occur simultaneously on faults, but at distinct scales.

The surfaces from laboratory experiments provide a test of an important implication of the minimum grooving scale. If the change from dominantly brittle to plastic deformation as a function of scale defines the asperity size that governs the frictional behavior, the friction as a function of slip should also change at this scale. When the fault slides, plastically flattened contacts weld and need to be sheared first (Engelder and Scholz, 1976; Dieterich, 1979; Dieterich and Kilgore, 1994; Marone, 1998). The critical slip distance L_c needed to shear the welded contacts should be the distance D_c over which friction evolves from its static to dynamic values, or more generally in rate-state friction, to a new steady-state value upon a sudden change in sliding velocity (Dieterich, 1979). The data set here includes surfaces from velocity stepping friction experiments that measured D_c. The values of L_c and D_c are similar in all cases. For the limestone experiments, D_c is 100 μm (Tisato et al., 2012), and L_c is 7–80 μm; for the clay-rich and serpentinite experiments, D_c is 19–69 μm, and L_c is 4–30 μm (Fig. DR13; Fig. 3B; Moore et al., 2012). The values of L_c = 4–500 μm on natural surfaces in Figure 3A are also suggestively close to extant laboratory measurements of D_c, which range from 1 to 100 μm (Marone, 1998; Tisato et al., 2012).

The interpretation of D_c as the scale of plastic deformation is an important clarification of the physical origins of D_c, which is commonly associated with an asperity refreshing distance. For a self-affine surface, asperity refreshing occurs at all scales, and therefore a specific process like the brittle-plastic transition is required to define a characteristic scale for frictional weakening.

The measurement of L_c and its interpretation as D_c are restricted to well-defined surfaces. Experiments demonstrate that slip weakening can accumulate over multiple surfaces, resulting in larger macroscopic slip weakening (Marone and Kilgore, 1993).

CONCLUSIONS

We have found a minimum scale of grooving. For each fault, the minimum grooving scale corresponds to a specific aspect ratio, and the fault is ungrooved at the scales over which the fault is relatively rough.

The new observation is useful for understanding the limits of one of the most common indicators of fault slip. The relationship to aspect ratio also invites an interpretation in terms of shear strain. At scales below the minimum grooving scale L_c, faults are sufficiently rough that asperities yield plastically. Values of the frictional slip weakening scale D_c are similar to the minimum grooving scale L_c. The scale D_c for solid surfaces is normally interpreted as a scale of asperity yield; plastic yielding combined with scale-dependent roughness define the process that sets the scale of the relevant asperities.

Faults certainly contain complications that are not captured in asperity-based models of solid friction. Other important processes include distributed deformation, fluid pressure, melting, chemical reactions, and granular flow. With all of these factors, it could be imagined that simple laboratory experiments of solid friction have no bearing on real faults. The observation of the minimum grooving scale suggests the opposite. There is a preserved fingerprint on natural fault surfaces of the fundamental process that governs solid friction. There may now be an observable connection between geological records of fault slip and the laboratory experiments on which our modern understanding of friction is based.

ACKNOWLEDGMENTS

We thank H. Savage and N. van der Elst for collecting the Mount St. Helens sample; and D. Moore, J. Hadizadeh, N. Tisato, M. Fondriest, T. Goebel, and the American Museum of Natural History for generously sharing laboratory data and samples. F. Renard, C. Thom, D. Goldsby, R. Carpick, and S. Siman-Tov provided helpful comments on early drafts. This work was funded in part by the Gordon and Betty Moore Foundation grant GBMF3289 to Brodsky.

REFERENCES CITED

Bowden, F.P., and Tabor, D., 1950, The Friction and Lubrication of Solids: Oxford, UK, Oxford University Press, 372 p.

Brace, W.F., 1963, Behavior of quartz during indentation: The Journal of Geology, v. 71, p. 581–595, doi:10.1086/626934.

Brodsky, E.E., Kirkpatrick, J.D., and Candela, T., 2016, Constraints from fault roughness on the scale-dependent strength of rocks: Geology, v. 44, p. 19–22, doi:10.1130/G37206.1.

Broz, M.E., Cook, R.F., and Whitney, D.L., 2006, Microhardness, toughness, and modulus of Mohs scale minerals: The American Mineralogist, v. 91, p. 135, doi:10.2138/am.2006.1844.

Candela, T., Renard, F., Klinger, Y., Mair, K., Schmittbuhl, J., and Brodsky, E.E., 2012, Roughness of fault surfaces over nine decades of length scales: Journal of Geophysical Research, v. 117, p. B08409, doi:10.1029/2011JB009041.

Dieterich, J., 1979, Modeling of rock friction: 1. Experimental results and constitutive equations: Journal of Geophysical Research, v. 84, p. 2161–2168, doi:10.1029/JB084iB05p02161.

Dieterich, J., and Kilgore, B., 1994, Direct observation of frictional contacts: New insights for state-dependent properties: Pure and Applied Geophysics, v. 143, p. 283–302, doi:10.1007/BF00874332.

Di Toro, G., Han, R., Hirose, T., De Paola, N., Nielsen, S., Mizoguchi, K., Ferri, F., Cocco, M., and Shimamoto, T., 2011, Fault lubrication during earthquakes: Nature, v. 471, p. 494–498, doi:10.1038/nature09838.

Engelder, J.T., and Scholz, C.H., 1976, The role of asperity indentation and ploughing in rock friction—II: Influence of relative hardness and normal load: International Journal of Rock Mechanics and Mining Sciences, v. 13, p. 155–163, doi:10.1016/0148-9062(76)90820-2.

Fang, Z., and Dunham, E.M., 2013, Additional shear resistance from fault roughness and stress levels on geometrically complex faults: Journal of Geophysical Research, v. 118, p. 3642–3654, doi:10.1002/jgrb.50262.

Fondriest, M., Smith, S., Candela, T., and Nielsen, S.B., 2013, Mirror-like faults and power dissipation during earthquakes: Geology, v. 41, p. 1175–1178, doi:10.1130/g34641.1.

Goebel, T.H.W., Candela, T., Sammis, C.G., Becker, T.W., Dresen, G., and Schorlemmer, D., 2013, Seismic event distributions and off-fault damage during frictional sliding of saw-cut surfaces with pre-defined roughness: Geophysical Journal International, doi:10.1093/gji/ggt401.

Greenwood, J.A., and Williamson, J.B.P., 1966, Contact of nominally flat surfaces: Proceedings of the Royal Society, Mathematical, Physical and Engineering Sciences, v. 295, p. 300–319, doi:10.1098/rspa.1966.0242.

Hyun, S., Pei, L., Molinari, J.F., and Robbins, M.O., 2004, Finite-element analysis of contact between elastic self-affine surfaces: Physical Review E, Statistical, Nonlinear, and Soft Matter Physics, v. 70, doi:10.1103/PhysRevE.70.026117.

Johnson, K.L., Greenwood, J.A., and Higginson, J.G., 1985, The contact of elastic regular wavy surfaces: International Journal of Mechanical Sciences, v. 27, p. 383–396, doi:10.1016/0020-7403(85)90029-3.

Lee, J.J., and Bruhn, R.L., 1996, Structural anisotropy of normal fault surfaces: Journal of Structural Geology, v. 18, p. 1043–1059, doi:10.1016/0191-8141(96)00022-3.

Lyell, C., 1871, The Student's Elements of Geology: New York, Harper & Brothers Publishers, 640 p.

MacElwane, J.B., 1936, Problems and progress on the geologico-seismological frontier: Science, v. 83, p. 193–198, doi:10.1126/science.83.2148.193.

Marone, C., 1998, Laboratory-derived friction laws and their application to seismic faulting: Annual Review of Earth and Planetary Sciences, v. 26, p. 643–696, doi:10.1146/annurev.earth.26.1.643.

Marone, C., and Kilgore, B., 1993, Scaling of the critical slip distance for seismic faulting with shear strain in fault zones: Nature, v. 362, p. 618–621, doi:10.1038/362618a0.

Moore, D.E., Lockner, D.A., Morrow, C.A., and Hickman, S., 2012, Frictional strengths of SAFOD core and Franciscan mélange samples at elevated temperatures: San Francisco, California, American Geophysical Union, Fall Meeting, abstract S11A-01.

Oliver, W.C., and Pharr, G.M., 1992, An improved technique for determining hardness and elastic-modulus using load and displacement sensing indentation experiments: Journal of Materials Research, v. 7, p. 1564–1583, doi:10.1557/JMR.1992.1564.

Oyen, M.L., and Cook, R.F., 2009, A practical guide for analysis of nanoindentation data: Journal of the Mechanical Behavior of Biomedical Materials, v. 2, p. 396–407, doi:10.1016/j.jmbbm.2008.10.002.

Power, W., and Tullis, T., 1991, Euclidean and fractal models for the description of rock surface roughness: Journal of Geophysical Research, v. 96, p. 415–424, doi:10.1029/90JB02107.

Renard, F., Voisin, C., Marsan, D., and Schmittbuhl, J., 2006, High resolution 3D laser scanner measurements of a strike-slip fault quantify its morphological anisotropy at all scales: Geophysical Research Letters, v. 33, p. L04305, doi:10.1029/2005GL025038.

Sagy, A., Brodsky, E.E., and Axen, G., 2007, Evolution of fault-surface roughness with slip: Geology, v. 35, p. 283–286, doi:10.1130/G23235A.1.

Scholz, C.H., 1988, The critical slip distance for seismic faulting: Nature, v. 336, p. 761–763, doi:10.1038/336761a0.

Siman-Tov, S., Aharonov, E., Sagy, A., and Emmanuel, S., 2013, Nanograins form carbonate fault mirrors: Geology, v. 41, p. 703–706, doi:10.1130/G34087.1.

Tisato, N., di Toro, G., de Rossi, N., Quaresimin, M., and Candela, T., 2012, Experimental investigation of flash weakening in limestone: Journal of Structural Geology, v. 38, p. 183–199, doi:10.1016/j.jsg.2011.11.017.

Verberne, B.A., Plumper, O., de Winter, D.A.M., and Spiers, C.J., 2014, Superplastic nanofibrous slip zones control seismogenic fault friction: Science, v. 346, p. 1342–1344, doi:10.1126/science.1259003.

Williams, J., 2005, Engineering Tribology: Cambridge, UK, Cambridge University Press, 488 p., doi:10.1017/CBO9780511805905.

Zum-Gahr, K.H., 1987, Microstructure and Wear of Materials: Amsterdam, Netherlands, Elsevier, 559 p.

Manuscript received 28 March 2016
Revised manuscript received 26 May 2016
Manuscript accepted 26 May 2016

Printed in USA